

Dynamical breaking of electron-hole symmetry in nonequilibrium chiral quantum channelsFelix Puster^{1,*}, Stefan G. Fischer², and Bernd Rosenow¹¹*Institut für Theoretische Physik, Universität Leipzig, Brüderstrasse 16, 04103 Leipzig, Germany*²*Institut für Nachhaltige Technische Systeme (INATECH), Universität Freiburg, 79110 Freiburg, Germany*

(Received 4 January 2024; accepted 1 February 2024; published 22 February 2024)

We investigate the relaxation dynamics in a chiral one-dimensional quantum channel with finite-range interactions, driven out of equilibrium by the injection of high-energy electrons. While the distribution of high-energy electrons, after dissipation of some of their energy, has been examined previously [Phys. Rev. B **108**, L081121 (2023)], we study the distribution of charge carriers excited from the channel's Fermi sea during this process. Utilizing a detector to measure the energetic imprint in the Fermi sea downstream of the injection point, we discover an initial symmetry in the distribution of excited electrons and holes relative to the Fermi level. However, this symmetry breaks down with stronger interactions and increased propagation distances, attributed to terms of order four and beyond in the interaction. We interpret these results in terms of interference between states with different numbers of plasmons in the Fermi sea.

DOI: [10.1103/PhysRevB.109.L081112](https://doi.org/10.1103/PhysRevB.109.L081112)

The complex relaxation dynamics in integrable systems offer an array of fascinating features that are not exclusively limited to thermal equilibration [1–4]. Certain experimental settings, such as trapped cold atoms prepared in specific nonequilibrium states, have demonstrated a lack of intrinsic relaxation [5,6]. By utilizing quantum wires, one can explore the relaxation dynamics inherent to the integrable Luttinger liquid model and beyond [7–13]. Additionally, quantum Hall edges, hosting chiral one-dimensional quantum channels, present us with further experimental opportunities for creating nonequilibrium states [14–18].

In the context of quantum Hall edges that contain multiple channels, considering contact interactions between electrons within these channels provides a sufficient description of relaxation phenomena [3,4,15,17,19–27]. The resulting dynamics yield nearly thermal metastable states, recently demonstrated in experimental setups [28,29]. These metastable states eventually thermalize on longer timescales, when nonlinear terms in the dispersion relation gain in importance and break integrability in the system [12,30–32].

For a comprehensive understanding of relaxation in single quantum Hall edge channels, it is necessary to consider finite-ranged interactions [21,24,33–36]. When the injection energy is below a specific threshold, dictated by the screening length and the interaction-renormalized Fermi velocity (the threshold becomes infinite for contact interactions), the Pauli blockade almost completely suppresses relaxation in these channels [21,35,37–39]. Above this energy threshold, the relaxation in single channels has recently been explored by considering electron injection at a defined high energy [40]. After an initial rapid decay, an unexpected cessation of energy relaxation was found, potentially attributable to an energy mismatch between

high-energy electrons and low-energy plasmons. This ultimately results in a metastable state that deviates significantly from equilibrium.

In this Letter, we focus on the investigation of excitations within the Fermi sea, which occur as a result of the relaxation of high-energy electrons in a single quantum Hall edge channel. To detect these excitations, we employ the resonant level of a quantum dot. The dot operates as a spectrometer for both electrons (above the Fermi level of the channel) and holes (below the Fermi level of the channel). These excitations can tunnel into a drain channel, as depicted in Fig. 1, thereby generating either a positive or negative detector current. The magnitude of this current corresponds to the density of the excitations, enabling us to quantify the perturbations within the channel, which are caused by the energy loss from the injected electron. An intriguing observation from our study is the development of an asymmetry in the densities of excited electrons and holes in the Fermi sea of the channel. This lack of symmetry is presumably induced by the interaction of the high-energy electron with the electrons in the Fermi sea. Due to this interaction, the state of the Fermi sea becomes a superposition of states with different numbers of plasmons. We interpret the asymmetry between particle and hole excitations in terms of interference between different states in the superposition, i.e., interference between states with different numbers of plasmons.

Model and Hamiltonian. High-energy electrons are injected into the chiral channel through an initial quantum dot, possessing a resonant level at energy ω_i (see Fig. 1). In a scenario with a high injection energy ($\omega_i \gg v/\lambda$), the detector signal resulting from the injected electrons that have dissipated some of their energy can be distinguished from the signal originating from charge carriers that are excited from the Fermi sea [40]. A subsequent quantum dot detects this signal at an energy level ω_f . While the signal from injected electrons at $\omega_f \approx \omega_i$ has been explored thoroughly in

*felix.puster@uni-leipzig.de

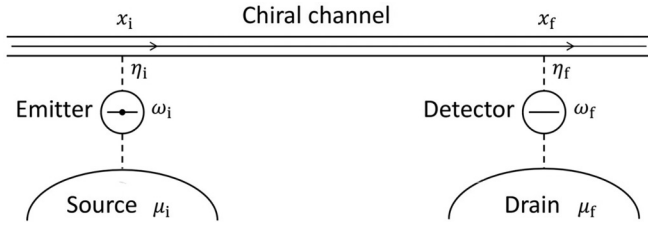


FIG. 1. Setup: Electrons with energy ω_i are injected from an emitter quantum dot into a chiral quantum channel, driving it out of equilibrium. The chemical potential of the source μ_i is set to ensure constant filling of the emitter quantum dot. The relaxation process of these injected electrons gives rise to excitations within the Fermi sea. After a specified propagation distance, these excitations are detected by a detector quantum dot. To ensure that only excitations are detected, the drain's chemical potential μ_f is chosen equal to the channel's chemical potential μ . The energy of the detector quantum dot ω_f is then varied to determine the density of the excitations.

Ref. [40], in this Letter, we examine the signal from charge carriers at $\omega_f \approx \mu$, which have been excited from the Fermi sea during the above-mentioned process.

In this analysis, we will limit our consideration to the case of small tunneling amplitudes ($\eta_{i/f}$). Utilizing the Keldysh formalism, we can treat the tunneling Hamiltonians

$$H_{t;i/f} = \eta_{i/f} \int dk e^{-ikx_{i/f}} c_k^\dagger d_{i/f} + e^{ikx_{i/f}} d_{i/f}^\dagger c_k, \quad (1)$$

in a perturbative manner up to the lowest nonvanishing order [41–43]. The quantum dots are described by the Hamiltonian $H_{\text{dot}} = \omega_i d_i^\dagger d_i + \omega_f d_f^\dagger d_f$, and the equilibrium electron system within the channel is characterized by the Hamiltonian

$$H = \int dk v k \hat{c}_k^\dagger \hat{c}_k + \frac{1}{4\pi} \int dk dk' dq v_q \hat{c}_{k-q}^\dagger \hat{c}_{k'+q}^\dagger \hat{c}_{k'} \hat{c}_k. \quad (2)$$

Here, v_q represents the Fourier transform of the real-space interactions between electrons. These interactions between the injected electrons and those already present in the channel lead to the excitation of plasmons within the Fermi sea of the channel.

Excess electron distribution. We start by bosonizing the Hamiltonian H in Eq. (2). This process provides us with formulas for the greater (+) and lesser (−) Green's functions of the channel, which can be expressed as $G^\pm(x, t) = G_0^\pm(x, t) \exp[S^\pm(x, t)]$. In this equation, $G_0^\pm(x, t) = 1/2\pi(x - vt \pm i\epsilon)$ represents the noninteracting component which is separated for convenience [35,40]. The influence of interactions is encapsulated in the exponent. Assuming a zero-temperature limit, this component can be defined by the following formula,

$$S^\pm(x, t) = \int_0^\infty \frac{dq}{q} [e^{\mp i(\omega_q t - qx)} - e^{\mp i(vqt - qx)}], \quad (3)$$

where $\omega_q = vq(1 + v_q/2\pi v)$ denotes the plasmon dispersion relation.

In the following, we examine interactions characterized by an exponential decay in momentum space, with screening length λ and strength ν [40], denoted by

$$v_q^{(\text{exp})} = \nu \exp(-\lambda|q|). \quad (4)$$

This representation allows us to approximate the corresponding Green's functions, thereby facilitating an analytical treatment and improving the efficiency of numerical evaluation.

Upon employing Eq. (4), the exponent in Eq. (3) can be expressed as a sum of powers of simple poles in the complex t plane [40],

$$S^{(\text{exp})\pm}(x, t) = \sum_{n=1}^{\infty} \frac{1}{n} \left[\frac{\frac{\nu}{2\pi} t}{x - vt \pm i\lambda n} \right]^n. \quad (5)$$

We also explore a model Green's function [35,40] which only contains two velocities instead of a continuum of plasmon velocities

$$G_{2v}^\pm(x, t) = \frac{1}{2\pi} \frac{1}{x - vt \pm i\epsilon} \frac{x - vt \pm i\lambda_c}{x - \bar{v}t \pm i\lambda_c}, \quad (6)$$

where one pole is determined by the unrenormalized electronic velocity v and another by the interaction renormalized velocity $\bar{v} = v + \nu/2\pi$, which coincides with the plasmon velocity defined by the derivative of ω_q at $q = 0$.

In both models, we enforce strict chirality, setting the advanced Green's function $G^a(x, t) = \Theta(-t)[G^<(x, t) - G^>(x, t)]$ to zero for $x > 0$. Assuming small tunneling amplitudes $\eta_{i/f}$, the general formula for the distribution of electrons and holes in relation to the channel's ground state [41–43] (which is proportional to the detector signal both above and below the Fermi level) can be expressed as follows:

$$\begin{aligned} p(x, \omega_i, \omega_f) &= \frac{v^2}{2\pi} \int_{-\infty}^{+\infty} dt_0 \int_{-\infty}^{+\infty} dt_1 \int_{-\infty}^{+\infty} dt_2 e^{i\omega_f t_0} e^{-i\omega_i(t_1 - t_2)} \\ &\times G^-(0, t_1 - t_2) G^a(0, -t_0) [\Pi^{++}(x, 0, t_0, t_1, t_2) \\ &- \Pi^{--}(x, 0, t_0, t_1, t_2)]. \end{aligned} \quad (7)$$

In this equation, α denotes the lesser component (−) below the Fermi level, $\omega_f < 0$, and the greater component (+) above the Fermi level, $\omega_f > 0$. In addition, we use the abbreviation $\Pi^{\beta\gamma}(x, t_0, t_1, t_2, t_3) = G^\beta(x, t_0 - t_3) G^\gamma(x, t_1 - t_2) / G^\beta(x, t_1 - t_3) G^\gamma(x, t_0 - t_2)$, and the distance $x = x_f - x_i$ describes the spatial separation between the emitter and detector along the channel.

Two-velocity model. To focus on the energetic sector of Fermi sea excitations centered around the chemical potential $\mu = 0$ for high-energy injected electrons ($\omega_i \gg \bar{v}/\lambda$), we will neglect the poles of the Green's functions in Eq. (7) that contribute to terms decaying exponentially with ω_i . This approach leads to the following expression for both models:

$$\begin{aligned} p_{\text{FS}}(x, \omega_f) &= -i \frac{v^2}{2\pi} \int_{-\infty}^{\infty} dt_0 \int_{-\infty}^{\infty} dt_1 e^{i\omega_f(t_0 - t_1)} \\ &\times G_c^\alpha(0, t_1 - t_0) \exp[S^+(x, t_0) - S^-(x, t_0)] \\ &\times \exp[S^-(x, t_1) - S^+(x, t_1)]. \end{aligned} \quad (8)$$

As a first test for the validity of Eq. (8), we apply it to the Green's functions of the two-velocity model specified in Eq. (6). This method leads to the following result for the

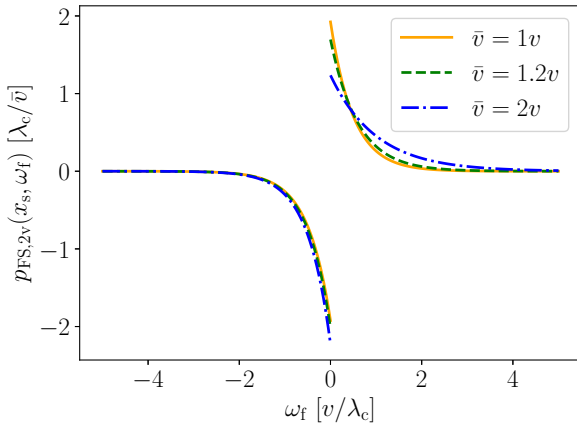


FIG. 2. Fermi sea distribution for the two-velocity model, evaluated at $x_s = 10\lambda_c$. The resulting distribution, as apparent from Eqs. (9) and (10), decays exponentially as a function of the detection energy. While the distribution is symmetric between positive and negative energies in the scaling limit $\bar{v} = v$ [cf. Eq. (11)], for $\bar{v} > v$ the distribution develops an asymmetry with a slower decay for $\omega_f > 0$, but a smaller initial value for $\omega_f = 0^+$ as compared to $\omega_f = 0^-$.

density of electrons above the Fermi sea ($\omega_f > 0$),

$$p_{\text{FS},2v}^e(x_s, \omega_f) = + \frac{\lambda_c x_s^2 + \lambda_c^2 (1 - \frac{\bar{v}}{v})^2}{\bar{v} x_s^2 + \lambda_c^2 (1 + \frac{\bar{v}}{v})^2} \left(\frac{4v}{3\bar{v}} + \frac{2}{3} \right) \exp\left(-2\omega_f \frac{\lambda_c}{\bar{v}}\right). \quad (9)$$

Similarly, we obtain the density of holes below the Fermi sea ($\omega_f < 0$) as

$$p_{\text{FS},2v}^h(x_s, \omega_f) = - \frac{\lambda_c x_s^2 + \lambda_c^2 (1 - \frac{\bar{v}}{v})^2}{\bar{v} x_s^2 + \lambda_c^2 (1 + \frac{\bar{v}}{v})^2} \frac{6}{(2 + \frac{\bar{v}}{v})} \exp\left(+2\omega_f \frac{\lambda_c}{v}\right). \quad (10)$$

Here, $x_s = (\bar{v} - v)x/v$ corresponds to the spatial dispersion of the wave packet when observed at the detection point [40]. The expressions in Eqs. (9) and (10), displayed for $x_s = 10\lambda_c$ in Fig. 2, agree with the results derived for the corresponding Fermi sea excitations when fully evaluating Eq. (7) for the two-velocity model [Eq. (6)]. This agreement holds true in the limit of high injection energy limit, i.e., when $\omega_i \gg \bar{v}/\lambda$ [40].

Distribution for exponential interaction. We set out to evaluate the distribution in Eq. (8) numerically for the full

interaction exponent specified in Eq. (5). This equation is the outcome of employing the exponential form of interactions found in Eq. (4). To achieve this, we consider a scaling limit characterized by large propagation distances ($x \gg \lambda$) and weak interactions ($v/2\pi \ll v$). We maintain the product of these quantities, denoted by $x_s = xv/2\pi v$, which corresponds to the spatial dispersion at the detection point, as constant [40]. The two-velocity solution [Eqs. (9) and (10)] in this limit exhibits symmetry between electrons and holes, expressed as

$$p_{\text{FS},2v}(\omega_f, x_s) = \alpha \frac{2\lambda_c}{v} \frac{x_s^2}{x_s^2 + 4\lambda_c^2} e^{-\alpha\omega_f \frac{2\lambda_c}{v}}. \quad (11)$$

Here, $\alpha = +1$ when above the Fermi sea ($\omega_f > 0$) and $\alpha = -1$ when below the Fermi sea ($\omega_f < 0$). Notably, the distribution just decays exponentially as a function of the detection energy ω_f for all x_s values.

For the full model's evaluation, we begin by recognizing that the Green's functions independent of x in Eq. (8) become noninteracting within the scaling limit. By shifting $\tilde{t}_0 \rightarrow \tilde{t}_0 + x/v$ and $\tilde{t}_1 \rightarrow \tilde{t}_1 + x/v$ in Eq. (8), the scaling limit can be applied to the x -dependent exponents, yielding

$$S^{(\text{exp})\pm} \left(x, t + \frac{x}{v} \right) \xrightarrow[\text{limit}]{\text{scaling}} \sum_{n=1}^{\infty} \frac{1}{n} \frac{(-x_s)^n}{(vt \mp i\lambda n)^n}. \quad (12)$$

By understanding the singularities of the integrand in Eq. (8), we are able to express the distribution as the limit of a sequence of contour integrals. The integrand of each element of the sequence is proportional to the integrand in Eq. (8) but with the sums in the exponent restricted to the first N terms. As a result, for each element of the sequence, the integrand has only a finite number of singularities. The integration contour we consider is given by a semicircle that follows the real line and is closed in the suitable half plane, encapsulating all singularities within that half plane. The contribution of the arc segment of the contour decreases in accordance with Jordan's lemma. For each sequence element, we can then separate the two contour integrals by rewriting the noninteracting Green's function as an integral

$$\frac{1}{v(\tilde{t}_0 - \tilde{t}_1) \pm i\epsilon} = \mp iv \int_0^{\infty} d\omega e^{\pm i\omega[(\tilde{t}_0 - \tilde{t}_1) \pm i\epsilon/v]}, \quad (13)$$

and then exchanging the contour integrals with the frequency integral. Finally, we can identify the decoupled contour integrals as complex conjugates of each other and thus express the distribution as

$$p_{\text{FS}}(x_s, \omega_f) \xrightarrow[\text{limit}]{\text{scaling}} \lim_{N \rightarrow \infty} \frac{\alpha}{4\pi^2} \int_0^{\infty} d\omega \left| \int_{C_N} dt e^{i(\omega_f + \omega)t} \exp\left(\sum_{n=1}^N \frac{(-x_s)^n}{n} \left[\frac{1}{(vt - i\alpha\lambda n)^n} - \frac{1}{(vt + i\alpha\lambda n)^n} \right] \right) \right|^2, \quad (14)$$

where C_N can be any bounded contour enclosing all N singularities in the upper half plane, and $\alpha = +1$ for the electron distribution ($\omega_f > 0$) and $\alpha = -1$ for the hole distribution ($\omega_f < 0$). This approach facilitates an efficient nu-

merical computation of excited charge carriers' distributions, extending to values of x_s up to 100λ . In our numerical calculations, we employ dimensionless variables $\xi_s = x_s/\lambda$ and $\epsilon_f = \omega_f\lambda/v$.

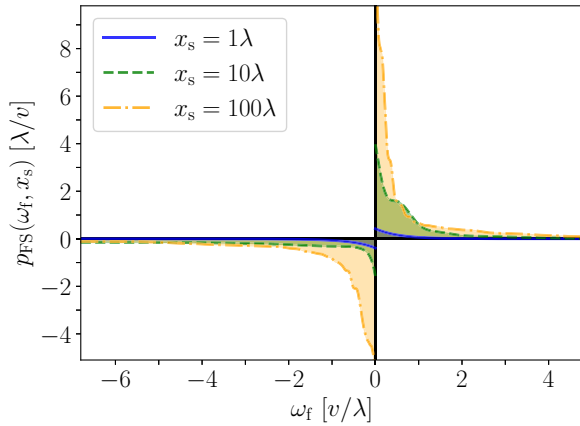


FIG. 3. Density p_{FS} of Fermi sea excitations for a range of x_s values. Interestingly, for large values of x_s , the distribution of excited electrons ($\omega_f > 0$) displays a greater concentration near the chemical potential at $\omega_f = 0$ compared to the distribution of holes ($\omega_f < 0$).

The distributions we have computed are presented in Fig. 3 for different values of x_s . It is apparent from Eq. (14) that, unlike the two-velocity model solution in the scaling limit, given in Eq. (11), the distributions of electrons and holes are not the same. This is due to the presence of α in the exponent. As shown in Fig. 3, an asymmetry develops between these distributions for larger x_s values. Contrary to the two-velocity model, the decay is not exponential as a function of detection energy. Instead, the hole distribution starts off with a slow decay, whereas the electron distribution has a higher peak at low energies before rapidly decaying.

This asymmetry is visualized in Fig. 4, which displays the difference, $|p_{\text{FS}}(\omega_f, x_s)| - |p_{\text{FS}}(-\omega_f, x_s)|$, between the absolute values of the electron and hole distributions at the corresponding x_s values. Notably, the distribution for $x_s = \lambda$ is almost symmetric. Close to the Fermi energy, it only deviates by a few percent from the two-velocity solution given in Eq. (11). This similarity to the two-velocity solution is even more pronounced for smaller x_s values.

By expanding Eq. (8) for the exponential interaction model in the scaling limit in x_s/λ and evaluating the integrals up to a specific order in x_s/λ , we gain insight into the similarity between the two solutions for small values of ξ_s . Numerically, we discover that the distribution is perfectly symmetric up to order $(x_s/\lambda)^2$. In an expansion, asymmetric contributions arise starting only at order $(x_s/\lambda)^4$ or higher. Consequently, the total distribution is nearly symmetric in the regime of weak interaction strength and short propagation length ($x_s/\lambda \leq 1$), which second-order perturbation theory adequately captures. We suggest that the asymmetric contributions at higher expansion orders arise due to the interference of states with different

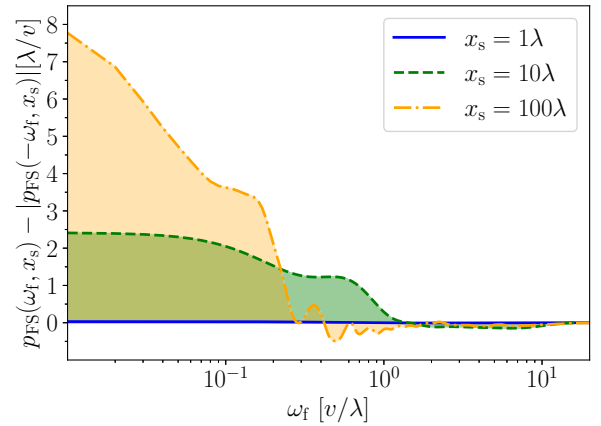


FIG. 4. The difference of Fermi sea excitation densities p_{FS} for electrons and holes, plotted for the same values of x_s in Fig. 3. For values $x_s \gg 1$, this difference becomes significant.

numbers of plasmons in the Fermi sea (cf. the discussion in the Supplemental Material [44]).

Additionally, we analytically derived the expansion up to order $(x_s/\lambda)^2$ and found that it matches the $(x_s/\lambda)^2$ term obtained from expanding Eq. (11) for small x_s when $\lambda_c = \lambda$. This clarifies why the two-velocity solution agrees well with the solution from the exponential interaction model for small x_s/λ values.

Conclusion. In this Letter, we have explored the excitation dynamics of charge carriers originating from the Fermi sea within a one-dimensional chiral channel, driven out of equilibrium by the dissipated energy of high-energy injected electrons. We focused on Fermi sea excitations by discarding terms that decay exponentially with the injection energy. We evaluated the robustness of this approach by juxtaposing the expression obtained by neglecting the exponentially decaying terms with the result of a full calculation of the channel's distribution and then taking the limit of high injection energy. This comparison was conducted within an analytical model that contains only two different excitation velocities.

Upon performing a numerical analysis of the densities of charge carriers excited from the Fermi sea for the full model within a scaling limit, we discovered an asymmetry between the excitations of electrons and holes. This asymmetry becomes apparent when the propagation distances and interaction strengths surpass the applicability of second-order perturbation theory.

Acknowledgments. F.P. acknowledges support by the Deutsche Forschungsgemeinschaft (DFG) under Grant No. 406116891 within the Research Training Group RTG 2522/1. B.R. acknowledges support by DFG RO 2247/11-1.

- [1] A. Polkovnikov, K. Sengupta, A. Silva, and M. Vengalattore, *Rev. Mod. Phys.* **83**, 863 (2011).
- [2] C. Gogolin and J. Eisert, *Rep. Prog. Phys.* **79**, 056001 (2016).
- [3] M. Millettari and B. Rosenow, *Phys. Rev. Lett.* **111**, 136807 (2013).

- [4] A. Schneider, M. Millettari, and B. Rosenow, *SciPost Phys.* **2**, 007 (2017).
- [5] T. Kinoshita, T. Wenger, and D. S. Weiss, *Nature (London)* **440**, 900 (2006).
- [6] S. Hofferberth, I. Lesanovsky, B. Fischer, T. Schumm, and J. Schmiedmayer, *Nature (London)* **449**, 324 (2007).

- [7] I. V. Lerner, V. I. Yudson, and I. V. Yurkevich, *Phys. Rev. Lett.* **100**, 256805 (2008).
- [8] A. Calzona, F. M. Gambetta, M. Carrega, F. Cavaliere, and M. Sassetti, *Phys. Rev. B* **95**, 085101 (2017).
- [9] A. Calzona, F. M. Gambetta, M. Carrega, F. Cavaliere, T. Schmidt, and M. Sassetti, *SciPost Phys.* **4**, 23 (2018).
- [10] A. Štrkalj, M. S. Ferguson, T. M. R. Wolf, I. Levkivskiy, and O. Zilberberg, *Phys. Rev. Lett.* **122**, 126802 (2019).
- [11] V. V. Deshpande, M. Bockrath, L. I. Glazman, and A. Yacoby, *Nature (London)* **464**, 209 (2010).
- [12] G. Barak, H. Steinberg, L. N. Pfeiffer, K. W. West, L. Glazman, F. von Oppen, and A. Yacoby, *Nat. Phys.* **6**, 489 (2010).
- [13] E. G. Idrisov and T. L. Schmidt, *Phys. Rev. B* **100**, 165404 (2019).
- [14] T. Krähenmann, S. G. Fischer, M. Rössli, T. Ihn, C. Reichl, W. Wegscheider, K. Ensslin, Y. Gefen, and Y. Meir, *Nat. Commun.* **10**, 3915 (2019).
- [15] R. H. Rodriguez, F. D. Parmentier, D. Ferraro, P. Roulleau, U. Gennser, A. Cavanna, M. Sassetti, F. Portier, D. Mailly, and P. Roche, *Nat. Commun.* **11**, 2426 (2020).
- [16] H. Kamata, T. Ota, K. Muraki, and T. Fujisawa, *Phys. Rev. B* **81**, 085329 (2010).
- [17] H. le Sueur, C. Altimiras, U. Gennser, A. Cavanna, D. Mailly, and F. Pierre, *Phys. Rev. Lett.* **105**, 056803 (2010).
- [18] C. Altimiras, H. le Sueur, U. Gennser, A. Cavanna, D. Mailly, and F. Pierre, *Nat. Phys.* **6**, 34 (2010).
- [19] D. Ferraro, B. Roussel, C. Cabart, E. Thibierge, G. Fève, C. Grenier, and P. Degiovanni, *Phys. Rev. Lett.* **113**, 166403 (2014).
- [20] M. Acciai, A. Calzona, G. Dolcetto, T. L. Schmidt, and M. Sassetti, *Phys. Rev. B* **96**, 075144 (2017).
- [21] C. Cabart, B. Roussel, G. Fève, and P. Degiovanni, *Phys. Rev. B* **98**, 155302 (2018).
- [22] P. Degiovanni, C. Grenier, G. Fève, C. Altimiras, H. le Sueur, and F. Pierre, *Phys. Rev. B* **81**, 121302(R) (2010).
- [23] A. M. Lunde, S. E. Nigg, and M. Buttiker, *Phys. Rev. B* **81**, 041311(R) (2010).
- [24] D. L. Kovrizhin and J. T. Chalker, *Phys. Rev. B* **84**, 085105 (2011).
- [25] I. P. Levkivskiy and E. V. Sukhorukov, *Phys. Rev. B* **85**, 075309 (2012).
- [26] A. O. Slobodeniuk, E. G. Idrisov, and E. V. Sukhorukov, *Phys. Rev. B* **93**, 035421 (2016).
- [27] H. Duprez, E. Sivre, A. Anthore, A. Aassime, A. Cavanna, A. Ouerghi, U. Gennser, and F. Pierre, *Phys. Rev. X* **9**, 021030 (2019).
- [28] H. Inoue, A. Grivnin, N. Ofek, I. Neder, M. Heiblum, V. Umansky, and D. Mahalu, *Phys. Rev. Lett.* **112**, 166801 (2014).
- [29] K. Itoh, R. Nakazawa, T. Ota, M. Hashisaka, K. Muraki, and T. Fujisawa, *Phys. Rev. Lett.* **120**, 197701 (2018).
- [30] A. Imambekov and L. I. Glazman, *Science* **323**, 228 (2009).
- [31] A. Imambekov, T. L. Schmidt, and L. I. Glazman, *Rev. Mod. Phys.* **84**, 1253 (2012).
- [32] T. Karzig, L. I. Glazman, and F. von Oppen, *Phys. Rev. Lett.* **105**, 226407 (2010).
- [33] P. Degiovanni, C. Grenier, and G. Fève, *Phys. Rev. B* **80**, 241307(R) (2009).
- [34] J. T. Chalker, Y. Gefen, and M. Y. Veillette, *Phys. Rev. B* **76**, 085320 (2007).
- [35] C. Neuenhahn and F. Marquardt, *New J. Phys.* **10**, 115018 (2008).
- [36] C. Neuenhahn and F. Marquardt, *Phys. Rev. Lett.* **102**, 046806 (2009).
- [37] M. Heyl, S. Kehrein, F. Marquardt, and C. Neuenhahn, *Phys. Rev. B* **82**, 033409 (2010).
- [38] T. Karzig, Low dimensional electron systems out of equilibrium, Dissertation, Freie Universität Berlin, 2012.
- [39] S. G. Fischer, J. Park, Y. Meir, and Y. Gefen, *Phys. Rev. B* **100**, 195411 (2019).
- [40] S. G. Fischer, Y. Meir, Y. Gefen, and B. Rosenow, *Phys. Rev. B* **108**, L081121 (2023).
- [41] C. L. Kane and M. P. A. Fisher, *Phys. Rev. B* **67**, 045307 (2003).
- [42] S. Takei, M. Milletari, and B. Rosenow, *Phys. Rev. B* **82**, 041306(R) (2010).
- [43] C. Han, J. Park, Y. Gefen, and H.-S. Sim, *Nat. Commun.* **7**, 11131 (2016).
- [44] See Supplemental Material at <http://link.aps.org/supplemental/10.1103/PhysRevB.109.L081112> for a discussion of how even interference between one- and two-plasmon states can lead to an asymmetric distribution.